

Magnetic resonance imaging of placental intralobule structure and function in a preclinical nonhuman primate model[†]

Andrew Melbourne^{1,2}, Matthias C. Schabel^{3,4}, Anna L. David² and Victoria H.J. Roberts^{5,*}

- ¹School of Biomedical Engineering and Imaging Sciences, King's College London, London, UK
- ²Department of Obstetrics and Maternal Fetal Medicine, Elizabeth Garrett Anderson Institute for Women's Health, University College London, London, UK
- ³Advanced Imaging Research Center, Oregon Health and Science University, Portland, OR, USA
- ⁴Utah Center for Advanced Imaging Research, University of Utah, Salt Lake City, Utah, USA
- ⁵Division of Reproductive and Developmental Sciences, Oregon National Primate Research Center, Oregon Health and Science University, Portland, OR, USA
- *Correspondence: Division of Reproductive and Developmental Sciences, Oregon National Primate Research Center, Oregon Health and Science University, Portland, OR, 97006, USA. Tel: 503-346-5431; E-mail: robertsv@ohsu.edu
- [†] **Grant Support:** This work was funded by the National Institutes of Health awards: P51-OD-011092, R01 HD086331, R01 HD108833, R03 HD097116, RDSP K12 HD000849, DP1DA056493. ALD is supported by the National Institute for Health and Care Research University College London Hospitals Biomedical Research Centre.

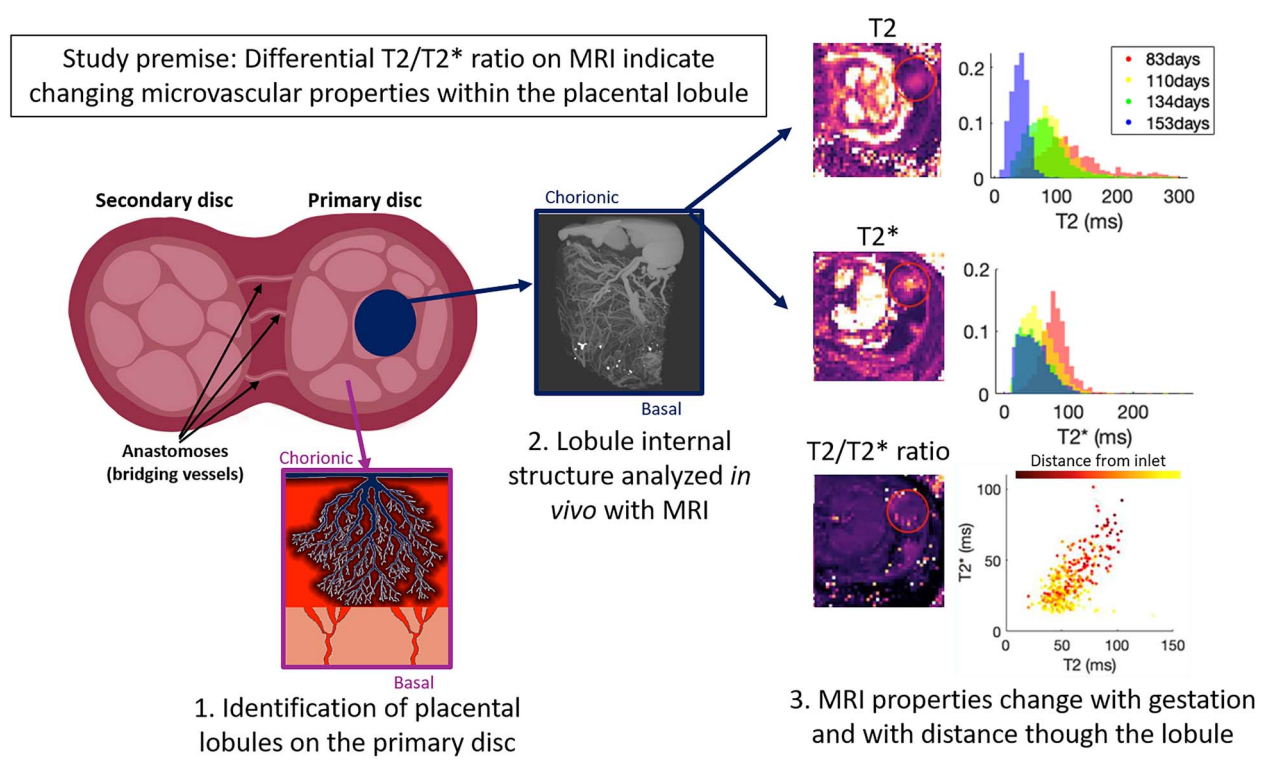
Abstract

Although the central role of adequate blood flow and oxygen delivery is known, the lack of optimized imaging modalities to study placental structure has impeded our understanding of its vascular function. Magnetic resonance imaging is increasingly being applied in this field, but gaps in knowledge remain, and further methodological developments are needed. In particular, the ability to distinguish maternal from fetal placental perfusion and the understanding of how individual placental lobules are functioning are lacking. The potential clinical benefits of developing noninvasive tools for the in vivo assessment of blood flow and oxygenation, two key determinants of placental function, are tremendous. Here, we summarize a number of structural and functional magnetic resonance imaging techniques that have been developed and applied in animal models and studies of human pregnancy over the past decade. We discuss the potential applications and limitations of these approaches. Their combination provides a novel source of contrast to allow analysis of placental structure and function at the level of the lobule. We outline the physiological mechanisms of placental T2 and T2* decay and devise a model of how tissue composition affects the observed relaxation properties. We apply this modeling to longitudinal magnetic resonance imaging data obtained from a preclinical pregnant nonhuman primate model to provide initial proof-of-concept data for this methodology, which quantifies oxygen transfer and placental structure across and between lobules. This method has the potential to improve our understanding and clinical management of placental insufficiency once validation in a larger nonhuman primate cohort is complete.

Summary Sentence

Here we overview existing MRI data acquisition methods and demonstrate our intention to uniquely combine these capabilities with newly developed analysis parameters in a translational animal model to advance our understanding of placental vascular function.

Graphical Abstract



Key words: placenta, fetal growth restriction, T2 relaxation, T2* relaxation, nonhuman primate.

Introduction

Magnetic resonance imaging (MRI) is a noninvasive method of interrogating anatomy and morphology, providing exquisite sensitivity to different tissue characteristics via contrast (both exogenous and endogenous) mechanisms that can be tuned via operator-specified instrument settings. Magnetic resonance imaging has found application in virtually every realm of biomedical imaging and organ systems. Over the past several decades, increasing emphasis has been placed on extending MRI from qualitative anatomic imaging, which dominated radiological applications, into the functional imaging domain, where the objective is the measurement and quantification of physiological parameters. These functional imaging methods have seen increasing application in fields as diverse as neuroimaging, cancer, and cardiac imaging. In the past decade, recognition of the importance of the placenta as a dynamic organ that grows and evolves over gestation and adapts to the needs of the developing fetus has spurred heightened interest in the development of MRI methods to detect aberrant placental development [1].

The placenta has a critical role in the delivery of oxygen and an array of nutrients, hormones, antibodies, and other biochemicals to the fetus, as well as the elimination of carbon dioxide and other waste products from the fetal circulation. Interrogating placental function is therefore essential for the assessment of fetal and maternal health during gestation. In the mature human placenta, the maternal-facing basal plate abuts the endometrium, with the center of each of the 20–30 lobules located over the opening of a maternal spiral artery. Maternal blood bathes the elaborately branched fetal villous

trees, each of which arises from a stem villus attached to the deep surface of the chorionic plate, with each maternal cotyledon occupied by several fetal villous trees [2–4]. Aberrant placental development has been linked with many adverse obstetric outcomes, including fetal growth restriction (FGR), preeclampsia, preterm labor, and stillbirth [5–8], and is implicated in a host of chronic and adult-onset health conditions, such as hypertension, diabetes, and dementia [9], with lifelong consequences for the offspring.

The placenta is unique in that it supports two independent circulations that do not mix: that of the fetus, which is intra-capillary and within the placental tissue; and that of the mother, which is (in humans) extra-vascular on arrival at the placental interface; blood moves slowly through the amorphous structure of the placental villous tissue within the intervillous space [2]. Exchange of oxygen and nutrients is maintained by passive diffusion or active transport across the villous syncytiotrophoblast, which forms a generally impermeable layer between the high oxygen saturation maternal circulation and the low oxygen saturation fetal circulation [10– 12]. Fetal and maternal blood thus see a different microvascular environment; this can be leveraged in MRI as the tissue properties are differentially affected, which facilitates analysis of the two vascular compartments. Differences manifest as variability in diffusion weighted imaging (DWI) properties and differential measurements of T2 and T2*, as described

In primates, maternal blood is supplied to the placenta via spiral arteries perfusing a sinus intervillous space rather than a capillary network. These spiral arteries pair with fetal villous

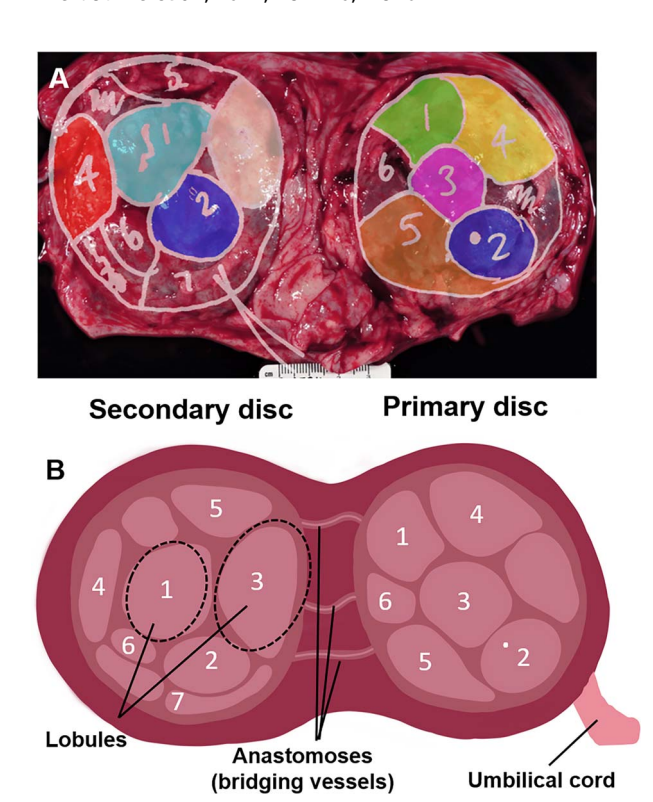


Figure 1. (A) Real-world mapping of identified placental lobules. Photograph of term placenta (basal side shown) with delineated placental lobules and color-coding shown overlaid. (B) Schematic diagram of the placenta demonstrating the anatomy of the two disks, the anastomoses, and lobules.

trees in functional cotyledons, with dozens of these cotyledons making up the complete placenta. Many of the placental MRI methodologies that have been applied to human pregnancies to date permit quantification of some aspects of placental perfusion, but with limited validation and do not account for the unique primate placenta structure. The nonhuman primate (NHP) provides a strong translational research animal model system for pregnancy studies due to the long gestational period, similar placentology, fetal physiology, and fetal growth trajectory [13]. Placentation in rhesus monkeys and humans is alike in several aspects, such as villous tree structure, the presence of an intervillous space, and the transformation of uterine spiral arteries as part of the establishment of the hemochorial placenta [14]. One key difference in structure is that macagues typically have a bidiscoid placenta rather than a single disk; the umbilical cord inserts into the primary disk, and anastomoses (bridging vessels) supply the fetal circulation to the structurally independent secondary disk [15]. The two disks function together as one unit but are anatomically distinct both on imaging and post-delivery gross inspection (Figures 1 and 2).

Although noninvasive MRI techniques have been established to a high level of sophistication for diagnostic imaging of fetal congenital and structural anomalies, the use of placental MRI is less well established. The following techniques are among those most developed.

Dynamic contrast-enhanced MRI (DCE) is a technique that makes use of an exogenous maternally delivered contrast injection to measure maternal-placental blood flow and intervillous volume [16–18]. In animal models, paramagnetic

gadolinium-based contrast agents that shorten T1 and T2 relaxation times are widely used [17]. Their application to the human placenta, however, is very limited due to concerns about the safety of these contrast agents in pregnancy, as they cross the placenta and accumulate in fetal tissues and have been associated with rheumatologic and inflammatory conditions and stillbirth when used after the first trimester. Iron-based paramagnetic contrast agents, which were first developed for the treatment of anemia, are also under investigation [19, 20].

Diffusion-weighted imaging and intra-voxel incoherent motion DWI (IVIM-DWI) are used to probe the villous microstructure, feto-placental microvasculature, and feto-placental blood volume [21–24].

Blood-oxygenation-level dependent MRI is an example of endogenous contrast that has been validated by our group in the NHP [25] and applied to human pregnancy studies [26] and has been used to measure the placental response to hyperoxia [17, 27–32]. Increasing maternal inhaled oxygen concentration has no safety concerns and is simple to perform during imaging.

Transverse relaxation-based image contrast is tightly coupled to blood oxygen concentration, such that average T2 [33] and T2* [26, 32, 34, 35] measurements both depend on the concentration of deoxyhemoglobin.

Other techniques, including arterial spin labeling [36, 37] and hyperpolarized gas imaging [38], have also been used and show promise for future developments in placental assessment.

Despite the proliferation of techniques, many of these measurements are difficult to interpret in terms of specific aspects of placental physiology [1]. Commonly reported whole-placenta average diffusivity, T2 and T2* values are not able to represent the complexity of the placental structure and do not explicitly measure oxygenation or blood flow, although some progress has been made in this area [39]. This is important as the function of each placental lobule may vary widely depending on its position, maturation, or even acquired damage through hemorrhage or infarction. Data acquisition techniques for these various MRI modalities are largely mature, but methods for analysis and interpretation of these data in the placenta remain incomplete. Approaches to coherently integrate multiple data sources in a self-consistent pipeline are also currently unavailable. Most significantly, placental MRI methods for assessment of perfusion and oxygen transport remain to be rigorously validated, and as a result, clinical applications of MRI for characterization of placental function remain largely phenomenological rather than quantitative.

Here, we outline the physiological mechanisms of T2 and T2* decay in the placenta and devise a model of how tissue composition affects the observed relaxation properties. T2* decay is rapid, comprising inhomogeneities of both the magnetic field and local tissue composition, facilitating fast imaging in the presence of motion, and is thus applicable to imaging a dynamic organ, such as the placenta, where motion may be caused by maternal breathing and fetal movement. Dephasing due to magnetic field inhomogeneities can be recalled with a spin-echo; there is no a priori reason for T2 \propto T2*, hence the two decay rates may contain different tissue information. We apply this modeling to longitudinal data obtained from a preclinical pregnant NHP model. These combined image acquisition and data modeling methods quantify

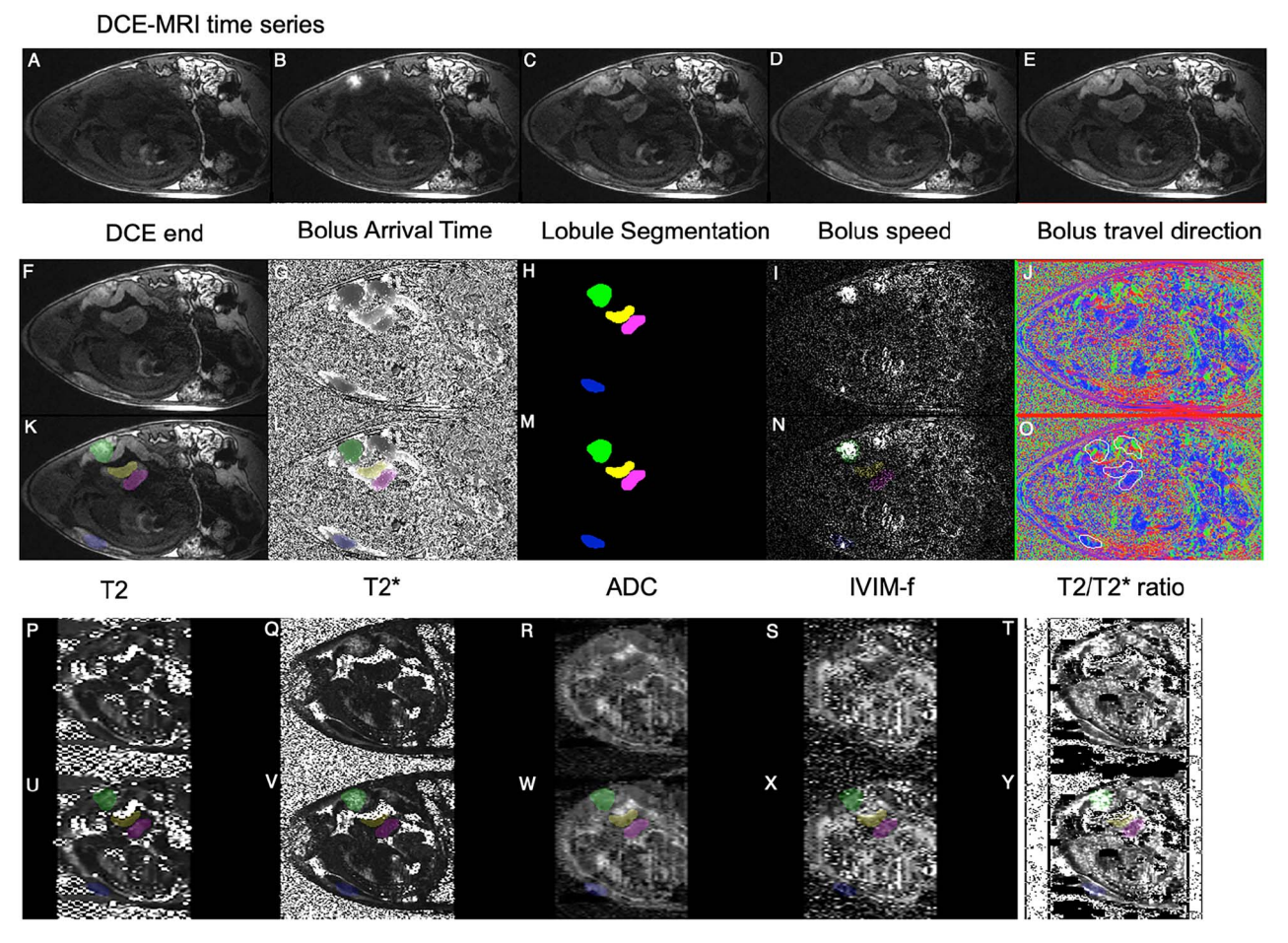


Figure 2. Example imaging data and fitted parametric mapping. (A–E) Example images from a DCE-MRI time-series showing contrast agent arrival (no scale). (F–J) Parametric mapping from DCE-MRI, including bolus arrival time (0–150 s) and segmentation; color-coded by lobule, see Figure 1. Panels (K–O), as for (F–J) with color-coded segmentation overlaid. Panels (P–T) show parametric maps from quantitative MRI for T2 (0–200 ms), T2* (0–200 ms), ADC ($0^{-4} \times 10^{-3}$ mm²s⁻¹), IVIM perfusion fraction (f, 0^{-1}), and T2*/T2 ratio. Panels (U–Y), as for (P–T) with segmentation overlaid.

oxygen transfer and placental structure across and between lobules, with potential to improve clinical management of placental insufficiency once validation studies in a larger NHP cohort are complete.

Methods

All experimental protocols were approved (Protocol #IP0001389) by the Institutional Animal Care and Use Committee (IACUC) of the ONPRC, and all procedures contributing to this work complied with the ethical standards of the relevant national guides on the care and use of laboratory animals from the Animal Welfare Act and were enforced by the United States Department of Agriculture.

Data and image acquisition

We acquired data from a single pregnant rhesus macaque over four gestational age (G) time points (days) corresponding to G83, G100, G134, and G153 (where the term is G165 days). Immediately following the last imaging study at G153, the pregnancy was delivered by cesarean section surgery for placenta collection, which included gross examination, mapping of lobules, weights, and measures, and extensive placental sampling for later use.

Magnetic resonance imaging studies were performed on an NHP-dedicated 3 T Siemens TIM-Trio scanner (Erlangen, Germany) using a circularly-polarized transmit, 15-channel receive radiofrequency (RF) "extremity" coil (QED, Cleveland, OH). Animals were maintained under constant anesthesia via an intravenous infusion of propofol along with cisatracurium, a paralytic agent, to eliminate residual motion from respiration. All imaging was performed during expiratory breath holding, achieved by temporarily suspending ventilation. Physiological monitoring of pulse rate, arterial blood oxygen saturation, and end-tidal CO₂ partial pressure was performed throughout each imaging study, with no deviations from normal ranges observed in these parameters.

After localization of the placenta and acquisition of T2-weighted half-Fourier acquisition single-shot turbo spin-echo anatomic images in the coronal and axial planes, axial 2D multislice spoiled gradient echo (SPGR) images (TR = 418 ms, flip angle = 30° , 256×72 matrix, 0.75 mm isotropic in-plane spatial resolution, 1.5 mm slice thickness) spanning the entire uterus were acquired at six in-phase echo times (TE = 4.92, 9.84, 19.68, 29.52, 36.90, and 44.28 ms) with monopolar readout gradients.

Two-dimensional multislice diffusion-weighted spin echo planar images (EPI) were acquired at multiple echo times and with multiple diffusion b-values as follows: b = 0/200 for 10

echo times (TE = 60, 80, 100, 120, 140, 160, 180, 200, 220, 280 ms) and TE = 67/120/180 ms for eleven *b* values (*b* = 0, 10, 20, 30, 40, 60, 80, 100, 200, 400, 800). These images were all acquired with a spatial resolution of $1.56 \times 1.56 \times 3.1$ mm.

Subsequently, 3D SPGR images were acquired in the coronal plane (TR = 5.1 ms, TE = 2.46 ms, 1.25 mm isotropic spatial resolution, flip angles of 2°, 3°, 5°, 10°, 25°, and 35°), also covering the entire uterus, to allow estimation of T1 (longitudinal relaxation time) with the variable flip angle (VFA) method. Immediately after acquisition of VFA data, 150 volumes of 3D SPGR images were acquired for DCE-MRI (TR = 2.66 ms, TE = 1.14 ms, flip angle = 20° , using TWIST undersampling with an acquisition time per frame of 2.74 s), with the field of view matched to the VFA images and a spatial resolution of $1.25 \times 1.25 \times 2.0$ mm. Five baseline images were acquired prior to sequential intravenous injection of 0.2 mL of ferumoxytol (Feraheme, AMAG Pharmaceuticals) followed by 1.2 mL of gadoteridol contrast reagent (Prohance, Bracco Diagnostics Inc., Princeton, NJ, USA) at a rate of 20 mL/min using a syringe pump (Harvard Apparatus, Holliston, MA, USA).

Model-fitting DCE-MRI analysis

Bolus arrival times can be measured from DCE-MRI placental analysis. The time to peak is a reliable measure of bolus arrival time and can be inferred from the time at which the peak gradient occurs [see Figure 2A–E showing the bolus passage at different times, and Figure 2G showing the relative estimated bolus arrival time (darker is earlier)]. The resulting maps can be used to delineate individual placental cotyledons (Figure 2H) and also provide some information about bolus speed (Figure 2I) and direction (velocity, Figure 2J). The lobule appearance is matched to information on placental lobule position mapped at cesarean section delivery, which in turn links to pathology (see Placental segmentation and registration). Correspondences between arrival time maps across gestational age allow the tracking of lobules at multiple gestational ages.

Apparent diffusion coefficient

Apparent diffusivity is measured with a log-linear fitting of the signal decay curve with increasing diffusion weighting. The basic equation for a single diffusion compartment is:

$$S(b) = S0 \exp(-b ADC)$$
.

The apparent diffusion coefficient (ADC) represents how quickly the MR signal decays with diffusivity. Signal is lost rapidly in high diffusion regions, such as fluid (amniotic fluid or cerebrospinal fluid) and less rapidly in cell-dense regions (placental tissue or cerebral white matter). Hence, the ADC represents some marker of cellular or structural density (Figure 2R).

T2 relaxometry

Estimates of T2 can be found by fitting a single-exponential decay curve to data from multiple echo times. If sufficient echo times are sampled, it is possible to fit multi-compartment models [21]. In this work, we have data from two echo times, which is fitted by a simple model inversion to simultaneously estimate the baseline signal S0 and the decay time T2. For two

echo times [t1, t2] and two signal measurements [S1, S2]:

$$T2 = (t2 - t1) / \log (S1/S2)$$
.

T2 has been found to be sensitive to tissue structure and oxygenation and has been shown to vary between different tissue compartments (fluid, maternal blood, fetal blood, and white and gray matter) (Figure 2P).

T2* relaxometry

Similar to Apparent diffusion coefficient section, estimates of T2* can be found by fitting a single-exponential decay curve to data at multiple echo times. For multiple echo times, the T2* can be estimated by log-linear least-squares fitting. The basic equation for a T2* decay is:

$$S(t) = S0 \exp(-t/T2^*)$$
.

The T2* is found by the log-linear fitting of log(S(t)) = log(S0) - t * (1/T2*) (where S0 is generally different between the sections above). T2* has been found to be highly sensitive to changes in maternal oxygenation [27, 40] (Figure 2Q).

IVIM fitting

Intra-voxel incoherent motion (IVIM) modeling assumes a model with two exponential decay components [41, 42]. The additional exponential component is used to capture signal decay that is too rapid to be described by ordinary Brownian motion and is ascribed to "perfusion" effects. In this case, linear model fitting is not possible, but non-linear modeling allows the extraction of a perfusion fraction. The standard IVIM model is as follows:

$$S(b) = S0 [f \exp(-d^* b) + (1 - f) \exp(-d b)]$$

where *f* represents a "perfusion" volume fraction of rapid signal decay (Figure 2S) and the fraction (1-*f*) represents the volume fraction of signal undergoing ordinary diffusion by temperature-dependent Brownian motion. This model can be biased if the T2 of the different compartments varies substantially [22].

Villous ratio = T2/T2*

Here, we present the results of the simple ratio above, to investigate how the proportionality of T2 and T2* changes within each lobule and with gestational age. Since T2 > T2* in biological material, this ratio is always greater than one. T2* decay is rapid, comprising magnetic field inhomogeneities well as local tissue composition inhomogeneities. Dephasing due to magnetic field inhomogeneities can be recalled with a spin-echo, and this slower T2 decay rate is thus less sensitive to local geometric features that influence the magnetic field, such as large vessels (Supplemental Figure S1). There is no a priori reason for T2 \propto T2*; hence, the two decay rates may contain different tissue information, and thus their combination may provide a novel source of endogenous contrast (see Figure 2T).

Placental segmentation and registration

Co-registration is a challenging prospect between EPI and SPGR, but intra-acquisition motion can be corrected by standard methods, and inter-acquisition methods appear relatively robust with respect to gross placental anatomy [43] assessed

through placental examination after birth. Figure 1 shows the lobule segmentation for primary and secondary disks for one animal. The same color-coding is used in all subsequent figures to identify individual lobules.

Segmentation is carried out for the latest gestational age (G153) on the DCE bolus arrival time image. These lobules are visually matched to the post-delivery image in Figure 2. Affine, followed by non-rigid image registration (niftyreg) [44], is used to map this segmentation to each earlier gestational age. Manual correction is used to preserve the lobule correspondence and to correct any residual misalignment with these earlier bolus arrival time images. This process ensures that we can establish a longitudinal correspondence during pregnancy between lobules within one subject.

Results

Parameter variability

Between primary and secondary disks

The macaque placenta ordinarily has two discrete disks. The umbilical cord inserts into the primary disk and is connected to a secondary disk via fetal chorionic bridging vessels. Typically, the secondary disk is smaller in volume, but there is substantial variability in the relative proportions [15]. The MR properties of each disk can be interrogated. We found no difference in segmented lobule volume or any of the five lobule-average MR parameters between the primary and secondary disks at any gestational age or in any parameter under Bonferroni correction for the 24 independent tests (four gestational time points, five MRI parameters, and volume) (Figure 3), suggesting no difference in the in vivo tissue properties of the primary and secondary disks. This is important for establishing how best to carry out subsequent post-delivery assessments of placental tissue.

Between segmented lobules

Each placental disk contains a discrete number of functional units, referred to as cotyledons or lobules, typically fewer than 10 per disk [15]. The lobule is the working unit of a primate placenta and so it is important to establish how tissue properties vary between these interchangeable units. Lobule segmentation in this animal revealed nine identifiable units, four on the primary disk, and five on the secondary disk. Figure 4 shows how tissue properties vary between the two disks. Some variability does exist, but broadly, the parameter distributions of each functional unit are indistinguishable for this normal placenta. Each lobule is color-coded according to its position identified in Figure 1.

Whole placenta distributions

Figure 5 shows the distribution of parameter values across all segmentations for all lobules and both disks. Distributions are generally unimodal. Due to the nature of the physical properties, negative values cannot occur for any of these markers. This means that the distributions are non-normal in appearance. The gamma distribution represents a reasonable distribution that maintains this non-negative property (shown overlaid). Normal distributions fit reasonably to ADC values, which have a tight positive distribution but are inappropriate for modeling either T2 or T2*.

Parameter changes within a lobule

Bolus arrival time as measured on DCE-MRI is a good indication of distance through a cotyledon. Lobules do not typically have a simple geometric arrangement (i.e., spherical), and so this represents a way to investigate how imaging properties vary within a lobule, independent of center-of-mass or Euclidean distance. Figure 6 shows how key quantitative imaging parameters vary with bolus arrival time through each lobule. Each lobule is color-coded according to its position identified in Figure 1 with the line of best fit shown.

Parameter changes through gestation

Figure 7 shows how imaging properties for each cotyledon change with increasing gestational age. Of note, the diffusion properties of ADC and IVIM perfusion fraction are relatively invariant with gestational age, but both T2 and T2* show strong decreases with gestational age, commensurate with what is known about placental oxygenation with gestation in primates. The overall trend lines (gray) in Figure 7 demonstrate high significance and a high negative correlation with gestational age for both T2 and T2* (but not for the remaining MRI parameters). Figure 8 shows the relationship between T2 and T2*, according to gestational age. There is evidence that the relationship between T2 and T2* varies through gestation. This may thus represent a novel marker of placental maturation, allowing an analysis of the separable effects of reversible and irreversible dephasing and their comparison to microstructural changes from ADC measurements.

Discussion

We have shown that quantitative imaging properties vary both within and between lobules across gestational age in the NHP placenta, a highly relevant animal model for human pregnancy. Our capability to delineate placental lobules and to use DCE-MRI to define a spatial-temporal relationship of imaging parameters through the lobule and across gestation is novel and demonstrates a proof-of-concept that may allow us to develop new systematic advances in placental imaging. Our preliminary results show that between lobule and between disk variability is low in this healthy macaque pregnancy and that substantial relationships are seen with gestational age, particularly in both T2 and T2*, in contrast to diffusionderived parameters. We also demonstrated that the ratio of T2/T2* is itself a potential future marker of placental function and maturation, allowing the separation of reversible and irreversible dephasing, and hence, the possible differentiation of the physiological effects giving rise to this difference. Although this ratio changes with gestational age, for this single animal, it remains fairly constant both within and between individual lobules.

The motivation for this work is the observation that the maternal and fetal blood compartments have different, but overlapping, diffusion, and relaxation properties. If the acquisition parameters sample these signal decay curves sufficiently, it is possible to disentangle the respective signal contributions from the separate blood pools. We anticipate that combining IVIM-DWI and T2/T2* will provide a clinically relevant method for measuring feto-placental oxygenation across a broad range of fetal oxygen saturations relevant to human FGR and that this methodology will be able to disentangle oxygenation changes from gestational tissue maturation

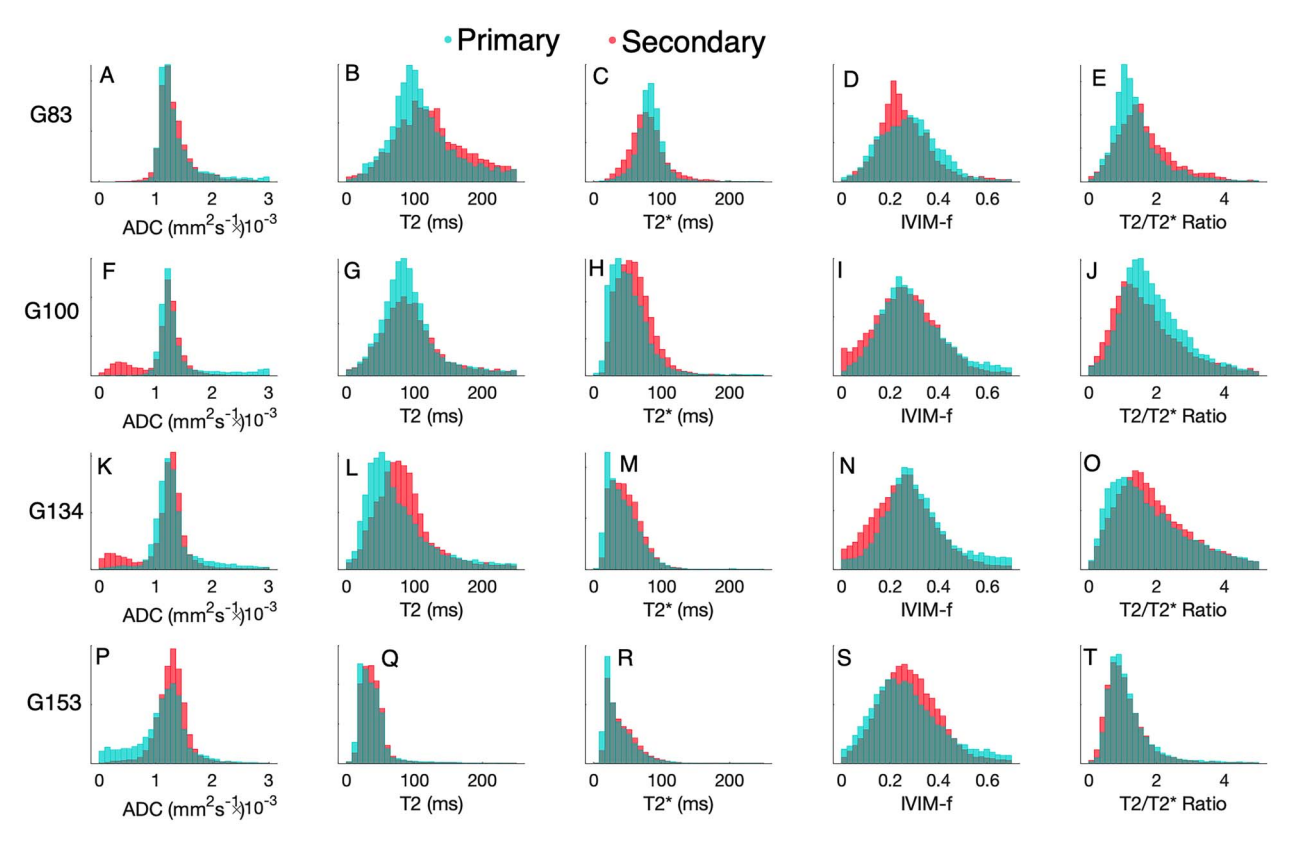


Figure 3. Comparison of quantitative mapping from MRI for lobules identified as primary disk (cyan) and secondary disk (red). Rows correspond to gestational age at MRI A-E 83 days, F-J 100 days, K-O 134 days, P-T 153 days.

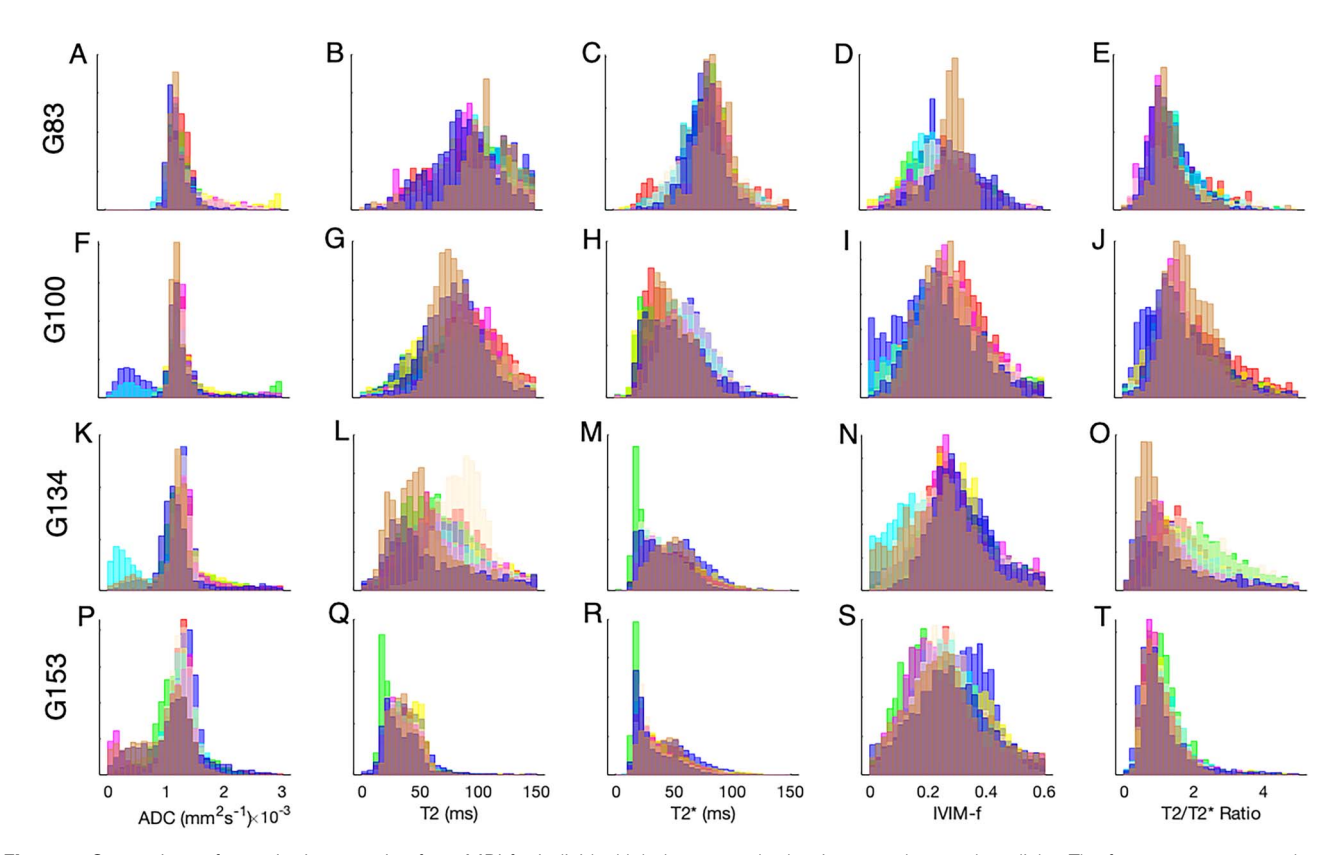


Figure 4. Comparison of quantitative mapping from MRI for individual lobules across both primary and secondary disks. The four rows correspond to gestational age at MRI: A-E 83 days, F-J 100 days, K-O 134 days, P-T 153 days. Color-coding corresponds with Figure 1.

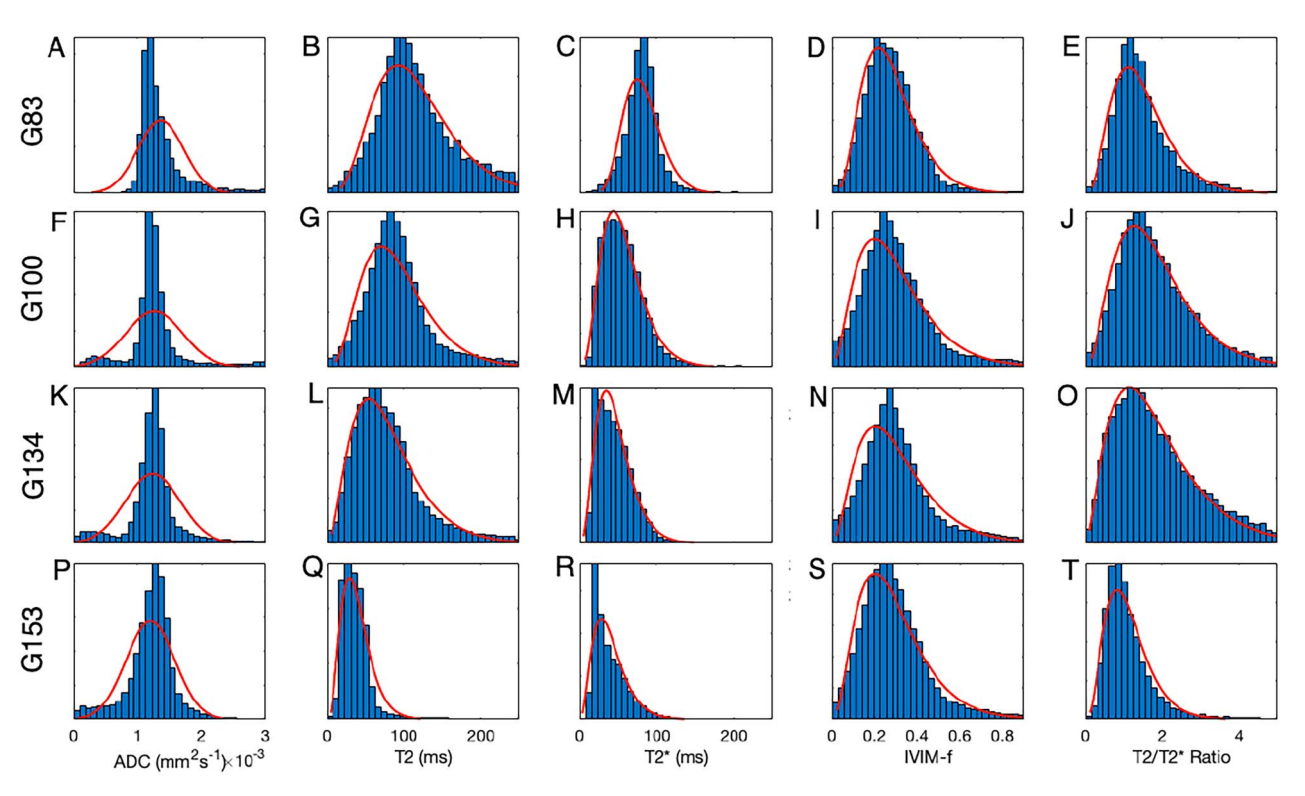


Figure 5. Comparison of quantitative mapping from MRI for whole placenta properties. The four rows correspond to gestational age at MRI: A-E 83 days, F-J 100 days, K-O 134 days, P-T 153 days. Results of normal and gamma distributions for fitting are shown overlaid.

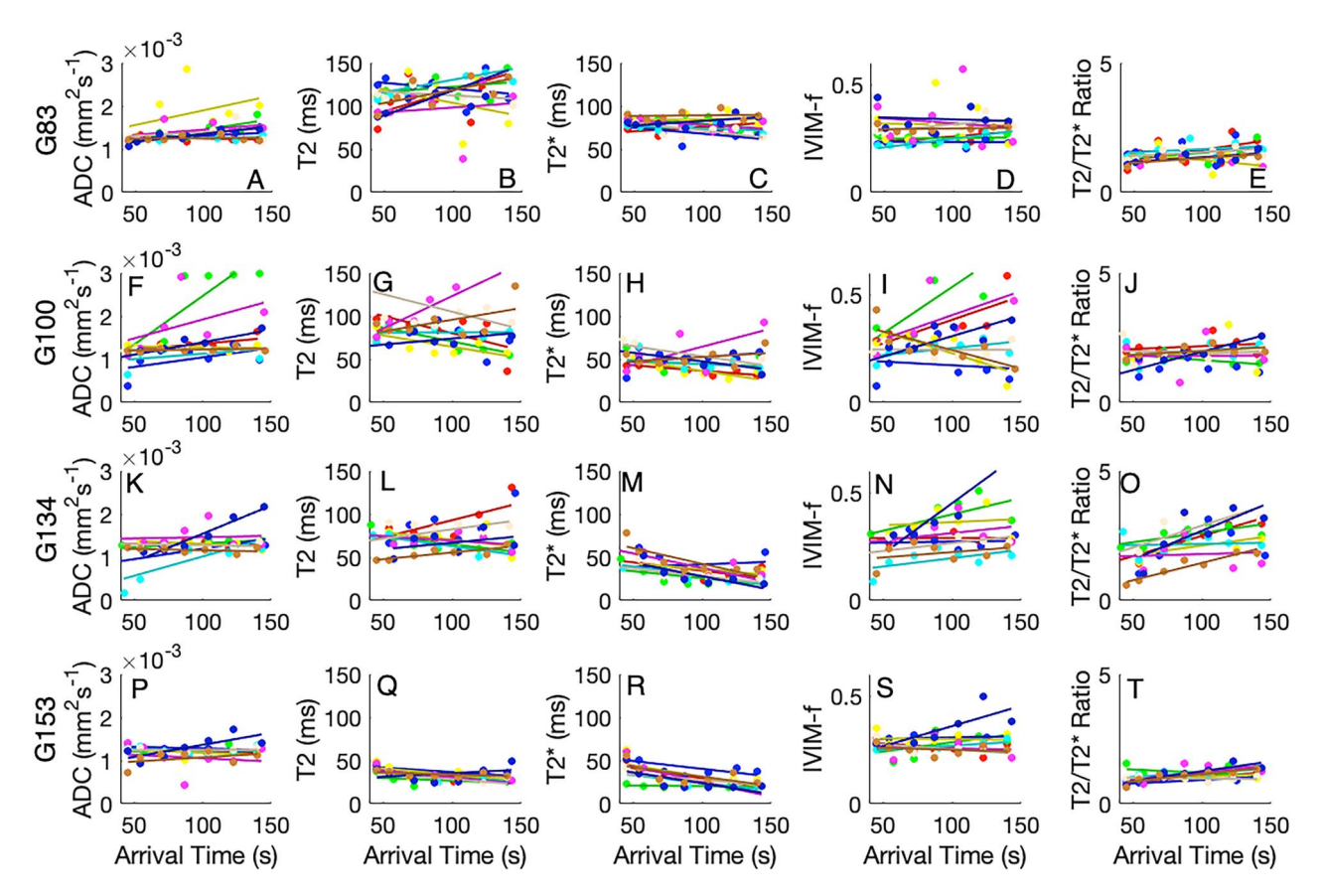


Figure 6. Variation of quantitative imaging parameters for each lobule with bolus arrival time as measured from DCE-MRI. The four rows correspond to gestational age at MRI: A-E 83 days, F-J 100 days, K-O 134 days, P-T 153 days. Color-coding corresponds with Figure 1.

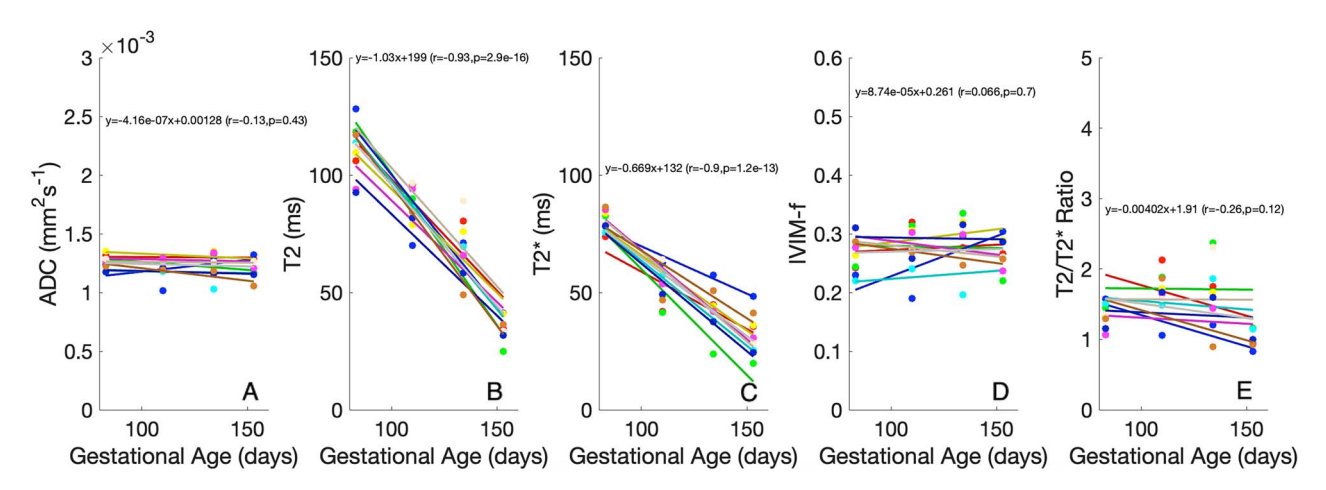


Figure 7. Variation of quantitative imaging parameters, A) ADC, B) T2, C) T2*, D) IVM-f and E) T2/T2* ratio for each lobule with gestational age. Color-coding corresponds with cotyledon position in Figure 1.

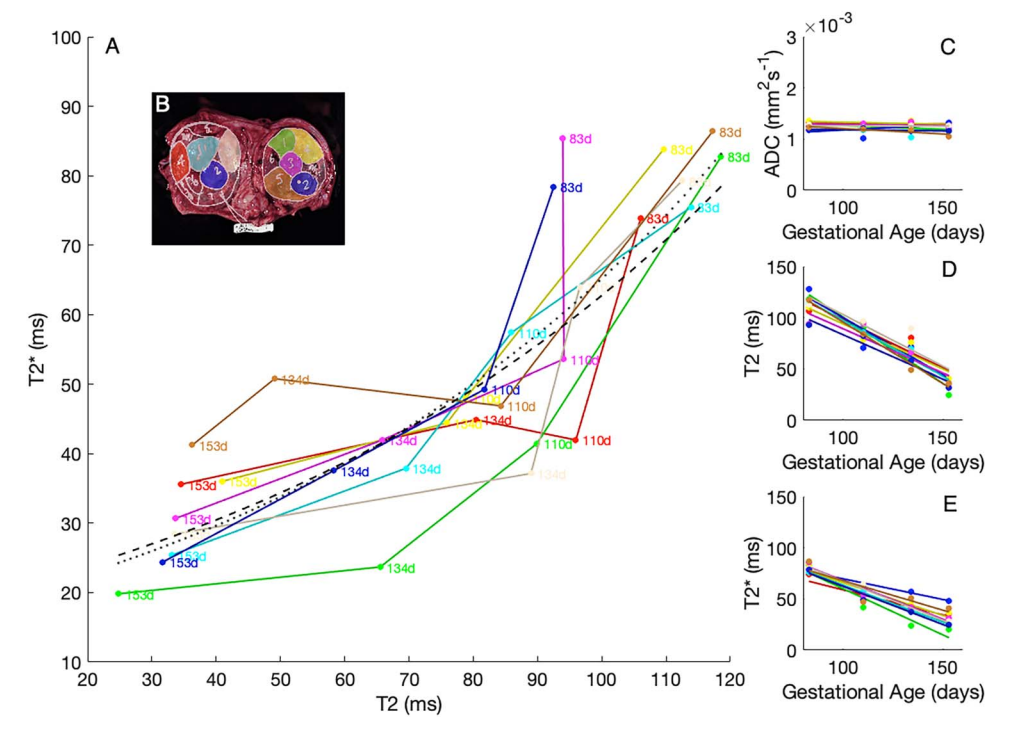


Figure 8. A) Variation of T2 and T2* with gestational age. Inset panels (C–E) show the independent parameter maps for ADC, T2, and T2*. Color-coding corresponds with cotyledon position in Figure 8B.

changes. For clinical application, systemic maternal contrast agents should be avoided due to concerns about their safety and potential adverse impact on fetal growth and development. The combination of IVIM-DWI and T2/T2* is a non-invasive method that allows separate measurement of the maternal and fetal compartments [39]. The simultaneous development of an optimized image acquisition protocol will support clinical adoption of these techniques.

There are limitations to the use of this experimental design. Although the NHP placenta is close to the human placenta in form and function, it does not recapitulate several pathologies that appear unique to humans, such as placental insufficiency leading to FGR, pre-eclampsia, and placental attachment disorders, such as placenta accreta. Nonetheless, the transfer of oxygen and nutrients to the fetus from an extra-vascular maternal space to a fetal capillary network is highly relevant.

Both the NHP and human placenta have discrete placental lobules, but our expectation is that these may be harder to characterize in humans due to their higher number, between 20 and 30 [2] compared to the 5–10 in the NHP placenta. The advantage of the preclinical NHP model is that it enables us to characterize individual lobule performance and to validate this experimentally. Analysis at the level of the lobule represents a distinct shift in how human placental imaging can be interpreted. The use of MRI for fetal and placental assessment will remain limited due to the cost and complexity of the procedure in comparison to ultrasound. However, the research capabilities of MRI and the ability to comprehensively study the structure and function of tissue will undoubtedly translate to new surrogate markers that can be obtained from more widespread ultrasound. Our use of DCE-MRI with exogenous contrast agents is made possible by the preclinical model. Dynamic contrast-enhanced MRI is widely considered the gold standard for vascular and perfusion imaging in MRI. Using the NHP model, we have performed two prior safety studies to demonstrate minimal transplacental transfer of gadolinium chelate to the fetus [45], with barely detectable levels in juvenile animals exposed to maternal gadolinium twice during mid to late gestation [46]. Nevertheless, our results shown here, describing links between DCE-MRI and other imaging contrasts, give us one possibility of moving away from gadolinium-based image contrast, which would be favorable for translation to human placental MRI implementation.

We have already demonstrated success in translating our NHP MRI and analysis tools to human pregnancies, both in women with normally grown fetuses and those with FGR due to placental insufficiency [47]. Furthermore, our work with T2* has already demonstrated high discriminatory power in prospectively identifying human pregnancies at risk of adverse pregnancy outcomes, such as pre-eclampsia and small gestational age [26]. Recent human studies using the combination of IVIM-DWI and T2/T2* have provided a physiological explanation for the known causative link between maternal supine sleeping and late gestation stillbirth, whereby supine position has an additive effect on the reduced fetal oxygen supply seen in FGR compared with normal pregnancies, rendering fetal oxygen supply even more insufficient [27, 48]. These studies support the generation of a validated quantitative model for joint IVIM-DWI and T2/T2* relaxometry, which could significantly improve assessments of perfusion and potentially characterize fetal oxygen saturation in vivo. There are several possible clinical use cases for this approach, as suggested below.

Fetal growth restriction

In the case of FGR mediated by placental insufficiency characterized by maternal villous malperfusion (MVM), poor maternal blood flow leads to poor perfusion to the intervillous space. These pregnancies present with abnormal uterine artery (UtA) Doppler waveforms, a small placenta, the presence of infarcts, and histologic abnormalities of the placental villi, including syncytial knot formation and distal villous hypoplasia [49]. Fetal blood oxygenation is low. In combination, this suggests that the maternal to fetal oxygen difference is large but with a low oxygen gradient since oxygen de-saturation is likely to occur progressively through the villous tree. T2 and T2* are both likely to be low in FGR with a characteristic gradient through placental lobules. Fetal vascular malperfusion may also present, either alone or in combination with MVM, where portions of the placental villous tree lack fetal vascular perfusion due to thrombus or cord occlusion. MRI assessment may be helpful here to determine how placental function is affected by poor fetal perfusion.

Poor oxygen transfer

Fetal growth restriction can also present despite normal UtA Doppler waveforms, with a diagnosis of massive perivillous fibrinoid deposition or chronic histiocytic intervillositis (CHI). Both conditions are rare but serious and are associated with recurrent late miscarriage, stillbirth, and FGR. An inflammatory disorder is believed to underlie these rare placental syndromes [50]. In the case of CHI, maternal blood is delivered to the intervillous space, but inflammatory processes with dense cellular infiltrates prevent oxygen

transfer across the trophoblast. Fetal blood oxygenation is again low as in FGR, but in this case the theoretical oxygen gradient is steeper since oxygen extraction is impeded. T2 and T2* are likely to be low as in FGR, but T2* is predicted to be differentially lower because of the enhanced oxygen gradient enhancing reversible dephasing in the maternal blood. A marker of placental structure sensitive to oxygen transfer and inflammation could provide new clinical avenues for testing new treatments in these conditions.

Poor oxygen carrying capacity (fetal anemia)

The effect of hematocrit on relaxation is important [2]. Since relaxation is dependent on the presence of deoxyhemoglobin, in the case of fetal anemia, a low hematocrit level in the fetus will limit the effect of deoxygenated fetal blood on the maternal blood pool. Both fetal and maternal T2 measurements will be theoretically higher, although this may be complicated by the ability of fetal blood cells to pick up oxygen and higher flow rates. Immediately after a fetal blood transfusion, hematocrit will rise and oxygen saturation will reach a short-term stable state. Imaging immediately before and after fetal transfusion should thus decouple differences in T2 and T2* since the maternal blood properties should be largely unaffected, and any effect on maternal blood would thus be caused by the influence of the change in fetal blood magnetic properties [51].

Conclusion

We have demonstrated the integration of in utero MR relaxometry and diffusion-weighted imaging in the NHP to quantify inter-lobule differences in tissue properties. This new combination of MRI methodologies and data modeling will provide a platform for future studies to investigate the relationships between placental blood flow and oxygenation with placental structural development, how it is altered by current therapeutics, and the investigation of emerging interventions in humans that attempt to modify abnormal placentation and mitigate adverse effects on the fetus. Once validated in our ongoing larger NHP cohort, this imaging methodology is anticipated to be highly amenable to subsequent optimization for clinical translation and may allow the effect of oxygenation changes to be investigated at an intra-placental level. Improved noninvasive diagnostics to identify pregnancies at risk of adverse outcomes due to placental dysfunction may allow for modification of clinical management plans.

Author contributions

Data acquisition (MCS and VHJR), Data analysis (MCS and AM), and Manuscript writing and editing (AM, VHJR, ALD, and MCS).

Supplementary material

Supplementary material is available at BIOLRE online.

Acknowledgment

We gratefully acknowledge Dr. Jamie Lo for support of the preliminary MRI animal data included in this manuscript which were acquired from an animal as part of a larger cohort study led by Dr. Lo.

Conflict of Interest: The authors have declared that no conflict of interest exists.

Data availability

The data underlying this article will be shared on reasonable request to the corresponding author.

References

- Guttmacher AE, Maddox YT, Spong CY. The human placenta project: placental structure, development, and function in real time. *Placenta* 2014; 35:303–304.
- 2. Burton GJ, Fowden AL. The placenta: a multifaceted, transient organ. *Philos Trans R Soc Lond B Biol Sci* 2015; 370:20140066.
- 3. Kaufmann P. Basic morphology of the fetal and maternal circuits in the human placenta. 1985; 13:5–17.
- 4. Huppertz B. The anatomy of the normal placenta. *J Clin Pathol* 2008; **61**:1296–1302.
- Kidron D, Bernheim J, Aviram R. Placental findings contributing to fetal death, a study of 120 stillbirths between 23 and 40 weeks gestation. *Placenta* 2009; 30:700–704.
- Roberts DJ, Post MD. The placenta in pre-eclampsia and intrauterine growth restriction. J Clin Pathol 2008; 61:1254–1260.
- Salafia CM, Vintzileos AM, Silberman L, Bantham KF, Vogel CA. Placental pathology of idiopathic intrauterine growth retardation at term. Am J Perinatol 1992; 9:179–184.
- Salafia CM, Vogel CA, Bantham KF, Vintzileos AM, Pezzullo J, Silberman L. Preterm delivery: correlations of fetal growth and placental pathology. *Am J Perinatol* 1992; 9:190–193.
- Andolf E, Bladh M, Möller L, Sydsjö G. Prior placental bed disorders and later dementia: a retrospective Swedish register-based cohort study. BJOG 2020; 127:1090–1099.
- Soothill PW, Nicolaides KH, Rodeck CH, Campbell S. Effect of gestational age on fetal and intervillous blood gas and acid-base values in human pregnancy. *Fetal Ther* 1986; 1:168–175.
- 11. Soothill PW, Nicolaides KH, Campbell S. Prenatal asphyxia, hyperlacticaemia, hypoglycaemia, and erythroblastosis in growth retarded fetuses. *Br Med J (Clin Res Ed)* 1987; **294**:1051–1053.
- Prinster A, Pierpaoli C, Turner R, Jezzard P. Simultaneous measurement of DeltaR2 and DeltaR2* in cat brain during hypoxia and hypercapnia. *Neuroimage* 1997; 6:191–200.
- 13. Benirschke K. Placentation. J Exp Zool 1983; 228:385-389.
- Carter AM. Animal models of human pregnancy and placentation: alternatives to the mouse. Reproduction 2020; 160:R129–R143.
- Roberts VHJ, Castro JN, Wessel BM, Conrad DF, Lewis AD, Lo JO. Rhesus macaque fetal and placental growth demographics: a resource for laboratory animal researchers. Am J Primatol 2023; 85:e23526.
- Frias AE, Schabel MC, Roberts VHJ, Tudorica A, Grigsby PL, Oh KY, Kroenke CD. Using dynamic contrast-enhanced MRI to quantitatively characterize maternal vascular organization in the primate placenta. Magn Reson Med 2015; 73:1570–1578.
- Chalouhi GE, Deloison B, Siauve N, Aimot S, Balvay D, Cuenod CA, Ville Y, Clément O, Salomon LJ. Dynamic contrast-enhanced magnetic resonance imaging: definitive imaging of placental function? Semin Fetal Neonatal Med 2011; 16:22–28.
- Siauve N, Chalouhi GE, Deloison B, Alison M, Clement O, Ville Y, Salomon LJ. Functional imaging of the human placenta with magnetic resonance. Am J Obstet Gynecol 2015; 213:S103–S114.
- Nguyen SM, Wiepz GJ, Schotzko M, Simmons HA, Mejia A, Ludwig KD, Zhu A, Brunner K, Hernando D, Reeder SB, Wieben O, Johnson K, et al. Impact of ferumoxytol magnetic resonance imaging on the rhesus macaque maternal-fetal interface. Biol Reprod 2020; 102:434–444.
- Zhu A, Reeder SB, Johnson KM, Nguyen SM, Fain SB, Bird IM, Golos TG, Wieben O, Shah DM, Hernando D. Quantitative ferumoxytol-enhanced MRI in pregnancy: a feasibility study in the nonhuman primate. *Magn Reson Imaging* 2020; 65:100–108.

- Melbourne A, Aughwane R, Sokolska M, Owen D, Kendall G, Flouri D, Bainbridge A, Atkinson D, Deprest J, Vercauteren T, David A, Ourselin S. Separating fetal and maternal placenta circulations using multiparametric MRI. Magn Reson Med 2019; 81: 350–361.
- 22. Jerome NP, d'Arcy JA, Feiweier T, Koh D-M, Leach MO, Collins DJ, Orton MR. Extended T2-IVIM model for correction of TE dependence of pseudo-diffusion volume fraction in clinical diffusion-weighted magnetic resonance imaging. *Phys Med Biol* 2016; 61:N667–N680.
- 23. Siauve N, Hayot PH, Deloison B, Chalouhi GE, Alison M, Balvay D, Bussières L, Clément O, Salomon LJ. Assessment of human placental perfusion by intravoxel incoherent motion MR imaging. J Matern Fetal Neonatal Med 2019; 32:293–300.
- Slator PJ, Hutter J, McCabe L, Gomes ADS, Price AN, Panagiotaki E, Rutherford MA, Hajnal JV, Alexander DC. Placenta microstructure and microcirculation imaging with diffusion MRI. *Magn Reson Med* 2018; 80:756–766.
- Schabel MC, Roberts VHJ, Lo JO, Platt S, Grant KA, Frias AE, Kroenke CD. Functional imaging of the nonhuman primate placenta with endogenous blood oxygen level-dependent contrast. *Magn Reson Med* 2016; 76:1551–1562.
- 26. Schabel MC, Roberts VHJ, Gibbins KJ, Rincon M, Gaffney JE, Streblow AD, Wright AM, Lo JO, Park B, Kroenke CD, Szczotka K, Blue NR, et al. Quantitative longitudinal T2* mapping for assessing placental function and association with adverse pregnancy outcomes across gestation. PloS One 2022; 17:e0270360.
- Abaci Turk E, Abulnaga SM, Luo J, Stout JN, Feldman HA, Turk A, Gagoski B, Wald LL, Adalsteinsson E, Roberts DJ, Bibbo C, Robinson JN, et al. Placental MRI: effect of maternal position and uterine contractions on placental BOLD MRI measurements. Placenta 2020; 95:69–77.
- 28. Francis ST, Duncan KR, Moore RJ, Baker PN, Johnson IR, Gowland PA. Non-invasive mapping of placental perfusion. *Lancet* 1998; 351:1397–1399.
- Moore LG, Charles SM, Julian CG. Humans at high altitude: hypoxia and fetal growth. Respir Physiol Neurobiol 2011; 178: 181–190.
- Ong SS, Tyler DJ, Moore RJ, Gowland PA, Baker PN, Johnson IR, Mayhew TM. Functional magnetic resonance imaging (magnetization transfer) and stereological analysis of human placentae in normal pregnancy and in pre-eclampsia and intrauterine growth restriction. *Placenta* 2004; 25:408–412.
- 31. Bonel HM, Stolz B, Diedrichsen L, Frei K, Saar B, Tutschek B, Raio L, Surbek D, Srivastav S, Nelle M, Slotboom J, Wiest R. Diffusion-weighted MR imaging of the placental in fetuses with placental insufficiency. *Radiology* 2010; 257:810–819.
- Sørensen A, Peters D, Fründ E, Lingman G, Christiansen O, Uldbjerg N. Changes in human placental oxygenation during maternal hyperoxia estimated by blood oxygen level-dependent magnetic resonance imaging (BOLD MRI). *Ultrasound Obstet Gynecol* 2013; 42:310–314.
- Derwig I, Barker GJ, Poon L, Zelaya F, Gowland P, Lythgoe DJ, Nicolaides K. Association of placental T2 relaxation times and uterine artery Doppler ultrasound measures of placental blood flow. *Placenta* 2013; 34:474–479.
- 34. Huen I, Morris DM, Wright C, Parker GJM, Sibley CP, Johnstone ED, Naish JH. R1 and R2* changes in the human placenta in response to maternal oxygen challenge. *Magn Reson Med* 2013; 70:1427–1433.
- Sørensen A, Peters D, Simonsen C, Pedersen M, Stausbøl-Grøn B, Christiansen OB, Lingman G, Uldbjerg N. Changes in human fetal oxygenation during maternal hyperoxia as estimated by BOLD MRI. Prenat Diagn 2013; 33:141–145.
- 36. Derwig I, Lythgoe DJ, Barker GJ, Poon L, Gowland P, Yeung R, Zelaya F, Nicolaides K. Association of placental perfusion, as assessed by magnetic resonance imaging and uterine artery Doppler ultrasound, and its relationship to pregnancy outcome. *Placenta* 2013; 34:885–891.

- Shao X, Liu D, Martin T, Chanlaw T, Devaskar SU, Janzen C, Murphy AM, Margolis D, Sung K, Wang DJJ. Measuring human placental blood flow with multidelay 3D GRASE pseudocontinuous arterial spin labeling at 3T. J Magn Reson Imaging 2018; 47: 1667–1676.
- Markovic S, Fages A, Roussel T, Hadas R, Brandis A, Neeman M, Frydman L. Placental physiology monitored by hyperpolarized dynamic 13C magnetic resonance. *Proc Natl Acad Sci U S A* 2018; 115:F2429–F2436.
- Flouri D, Darby JRT, Holman SL, Cho SKS, Dimasi CG, Perumal SR, Ourselin S, Aughwane R, Mufti N, Macgowan CK, Seed M, David AL, et al. Placental MRI predicts fetal oxygenation and growth rates in sheep and human pregnancy. Adv Sci (Weinh) 2022; 9:e2203738.
- Luo J, Abaci Turk E, Bibbo C, Gagoski B, Roberts DJ, Vangel M, Tempany-Afdhal CM, Barnewolt C, Estroff J, Palanisamy A, Barth WH, Zera C, et al. In vivo quantification of placental insufficiency by BOLD MRI: a human study. Sci Rep 2017; 7:3713.
- Le Bihan D, Breton E, Lallemand D, Grenier P, Cabanis E, Laval-Jeantet M. MR imaging of intravoxel incoherent motions: application to diffusion and perfusion in neurologic disorders. *Radiology* 1986; 161:401–407.
- 42. Flouri D, Owen D, Aughwane R, Mufti N, Maksym K, Sokolska M, Kendall G, Bainbridge A, Atkinson D, Vercauteren T, Ourselin S, David AL, et al. Improved fetal blood oxygenation and placental estimated measurements of diffusion-weighted MRI using data-driven Bayesian modeling. Magn Reson Med 2020; 83:2160–2172.
- Avants B, Tustison N, Song G. Advanced normalization tools (ANTS). *Insight J* 2008; 39:1014–1026.
- 44. Modat M, McClelland J, Ourselin S. Lung registration using the NiftyReg package. In: van Ginneken B (ed.), Medical Image

- Analysis for the Clinic: A Grand Challenge, Workshop Proc from MICCAI, Createspace Independent Publishing Platform, online book, vol. 2010. 2010.
- 45. Oh KY, Roberts VHJ, Schabel MC, Grove KL, Woods M, Frias AE. Gadolinium chelate contrast material in pregnancy: fetal biodistribution in the nonhuman primate. *Radiology* 2015; 276: 110–118.
- Prola-Netto J, Woods M, Roberts VHJ, Sullivan EL, Miller CA, Frias AE, Oh KY. Gadolinium chelate safety in pregnancy: barely detectable gadolinium levels in the juvenile nonhuman primate after in utero exposure. *Radiology* 2018; 286:122–128.
- 47. Aughwane R, Mufti N, Flouri D, Maksym K, Spencer R, Sokolska M, Kendall G, Atkinson D, Bainbridge A, Deprest J, Vercauteren T, Ourselin S, *et al.* Magnetic resonance imaging measurement of placental perfusion and oxygen saturation in early-onset fetal growth restriction. *BJOG* 2021; 128:337–345.
- 48. Jani D, Clark A, Couper S, Thompson JMD, David AL, Melbourne A, Mirjalili A, Lydon A-M, Stone PR. The effect of maternal position on placental blood flow and fetoplacental oxygenation in late gestation fetal growth restriction: a magnetic resonance imaging study. *J Physiol* 2023; 601:5391–5411.
- Kingdom JC, Audette MC, Hobson SR, Windrim RC, Morgen E. A placenta clinic approach to the diagnosis and management of fetal growth restriction. *Am J Obstet Gynecol* 2018; 218:S803–S817.
- Redline RW. Extending the Spectrum of massive perivillous fibrin deposition (maternal floor infarction). *Pediatr Dev Pathol* 2021; 24:10–11.
- 51. Xu J, Duan AQ, Marini D, Lim JM, Keunen J, Portnoy S, Sled JG, McCrindle BW, Kingdom J, Macgowan CK, Seed M. The utility of MRI for measuring hematocrit in fetal anemia. *Am J Obstet Gynecol* 2020; 222:81.e1–81.e13.